PHILOSOPHICAL TRANSACTIONS OF THE ROYAL SOCIETY A MATHEMATICAL, PHYSICAL & ENGINEERING SCIENCES

Hypersonic Flight Experience

Gerald D. Walberg

Phil. Trans. R. Soc. Lond. A 1991 **335**, 91-119
doi: 10.1098/rsta.1991.0038

Hypersonic flight experience

By Gerald D. Walberg

The George Washington University, Joint Institute for Advancement of Flight Sciences, NASA Langley Research Center, Hampton, Virginia 23665-5225, U.S.A.

The flight test results from the X-15, Asset, Prime, Reentry F and Shuttle Orbiter flight research programmes are reviewed and compared with theory and ground-based experiments. Primary emphasis is placed on our present capability to predict aerodynamic coefficients and stability derivatives, and distributions of surface pressure and aerodynamic heating rate for typical orbital and sub-orbital hypersonic vehicles. Overall, this comparison demonstrates the feasibility of designing hypersonic vehicles based on tests in conventional perfect-gas wind tunnels supplemented by state-of-the-art CFD analysis.

At Mach numbers up to approximately 8, real-gas effects are small and Mach number/Reynolds number simulation is sufficient to insure accurate prediction of aerodynamic characteristics. At higher mach numbers, real-gas effects become important but appear to affect primarily pitching moment and to have little influence on other aerodynamic characteristics. Viscous interaction effects appear to be well correlated by the viscous interaction parameter, $\bar{V}'_\infty$ and to affect primarily axial force. With the exception of RCS jet interactions, stability and control derivatives are well predicted throughout the hypersonic flight régime.

State-of-the-art aerodynamic heating techniques appear to give accurate predictions for laminar and fully turbulent attached flows so long as there are no strong shock interactions or non-equilibrium chemistry effects. For such flows, heating rate distributions depend only weakly on Mach number for $M_\infty \gtrsim 8$ and hence $M_\infty \approx 8$–10 wind tunnel results can be used throughout the hypersonic speed range. For high-speed, high-altitude flight, surface catalycity effects can have a major influence on heating rates but modern, finite-rate boundary layer analyses are capable of predicting major trends.

The major remaining challenges are the accurate prediction of: (1) real-gas effects on longitudinal trim, (2) the effectiveness of blended high altitude control systems, (3) shock interaction heating, (4) heating rates for separated vortex-dominated leeside flows, and (5) boundary layer transition and relaminarzation.

Finally, it is pointed out that there are no flight data on the propulsion–airframe integration effects that are so important for airbreathing launch vehicles.

1. Nomenclature

b	wing span
C_{A}	axial force coefficient
C_{D}	drag coefficient
C_{L}	lift coefficient
$\Delta C_{l,\mathrm{JI}}$	increment in rolling moment coefficient due to jet interaction effects

Phil. Trans. R. Soc. Lond. A (1991) **335**, 91–119
Printed in Great Britain

$C_{l_{\delta a}}$	rolling moment due to aileron deflection, $\partial C_l/\partial \delta a$
C_{m}	pitching moment coefficient
C_{m_δ}	pitching moment due to elevator deflection, $\partial C_{\mathrm{m}}/\partial \delta$
C_{n_β}	yawing moment due to sideslip, $\partial C_{\mathrm{n}}/\partial \beta$
C_{p}	pressure coefficient
$\Delta C_{Y,\mathrm{JI}}$	increment in sideforce coefficient due to jet interaction effects
c	wing chord
D	drag
H	local heat transfer coefficient
H_{ref}	reference heat transfer coefficient
h	altitude
k	roughness height
$\bar{k}$	recombination rate coefficient
L	lift
l	vehicle length
M	Mach number
$\dot{m}$	mass flow rate
p	static pressure
q	dynamic pressure
$\dot{q}$	heating rate
$\dot{q}_{\mathrm{ref}}$	reference heating rate
Re	Reynolds number
$Re_{k,T}$	roughness Reynolds number at the onset of transition
$Re_{x,T}$	local wetted-length Reynolds number at the onset of transition
r_{n}	nose radius
T	temperature
$\bar{T}$	dimensionless temperature, $T_{\mathrm{w}}/[\rho_\infty V_\infty^3/2\sigma]^{\frac{1}{4}}$
t	time
V	velocity
V_{orb}	orbital velocity
$\bar{V}'_\infty$	viscous interaction parameter (equations (1)–(3))
x	wetted length from stagnation point or wing leading edge
y	spanwise distance from vehicle centreline
β	angle of sideslip
α	angle of attack
δa	aileron deflection angle
γ	ratio of specific heats
γ_{e}	effective ratio of specific heats
ρ	density
σ	Stephan–Boltzmann constant

Subscripts

e	evaluated at boundary-layer edge
i	initial conditions
j	RCS jet
max	maximum value obtained during entry
ref	evaluated at the stagnation point of a 0.3 radius sphere
s	stagnation point
trim	aerodynamically trimmed

w evaluated at vehicle surface
∞ free stream

2. Introduction

The ultimate validation of hypersonic design techniques, be they theoretical or based on wind tunnel tests, must come from hypersonic flight data. Over the years there have been a number of hypersonic flight test programmes and taken together they provide a large, and in some ways, definitive, flight database. It is the purpose of the present paper to review the various hypersonic flight programmes and, by comparison with ground based experiment and theory, to identify those flight domains in which current design techniques may be used with confidence as well as those where complex aerothermodynamic phenomena remain difficult to predict. The emphasis of the present paper is on our ability to predict aerodynamic coefficients and stability derivatives and the distributions of external pressure and aerodynamic heating rate for typical orbital and sub-orbital hypersonic vehicles. Hence, only a portion of our hypersonic flight experience is addressed. There are, of course, other flight test results, such as structural and materials response, and control system and flying qualities evaluations which are also important. Readers interested in these aspects of hypersonic flight will find valuable information in the cited references.

3. Flight domains and aerothermodynamic phenomena

The present paper addresses hypersonic flight data pertinent to winged re-entry gliders such as the Shuttle Orbiter, Buran and Hermes, and air-breathing launch vehicles such as HOTOL, Sanger and NASP. Typical flight domains for these vehicles are presented in figure 1*a* along with contours of Mach number, Reynolds number and viscous interaction parameter, $\bar{V}'_\infty$. These flight domains are also presented in figure 1*b* along with thresholds which indicate the onset of various aerothermodynamic phenomena. The heavy, nearly vertical contours indicate the onset of oxygen and nitrogen dissociation and ionization for air in chemical equilibrium behind a normal shock wave. The horizontal dashed lines indicate the approximate altitudes at which departures from chemical equilibrium and continuum flow become significant. The heating-rate contours indicate the approximate velocity–altitude régimes where convective aerodynamic heating becomes important. By inspection of figure 1, the significant phenomena for each vehicle class can be identified.

(*a*) *Winged re-entry gliders*

As shown in figure 1, these vehicles fly at hypersonic mach numbers up to 30. For characteristic lengths typical of the Shuttle Orbiter and Buran (*ca.* 30 m), hypersonic Reynolds numbers range from 3×10^5 to 3×10^7. Because of their smaller size ($l \approx 15$ m), Hermes and the Japanese HOPE (H-II orbital plane) will fly through Reynolds numbers about half those of the Shuttle. These vehicles will experience viscous interaction parameter values from 10^{-1} to 10^{-3} as their altitude decreases from around 100 km to 40 km. If it is assumed that significant regions of turbulent flow can exist when $Re_\infty > 5 \times 10^6$, then vehicles flying near the lower bound of the re-entry glider flight domain would be expected to experience turbulent heat transfer near or shortly after the time of peak stagnation-point heating (i.e. $V \approx 0.8\ V_{\mathrm{orb}}$). On the other hand, vehicles flying near the upper bound might not experience turbulent heating at all. Similarly, if it is assumed that significant viscous interaction effects

PHILOSOPHICAL TRANSACTIONS OF THE ROYAL SOCIETY A MATHEMATICAL, PHYSICAL & ENGINEERING SCIENCES

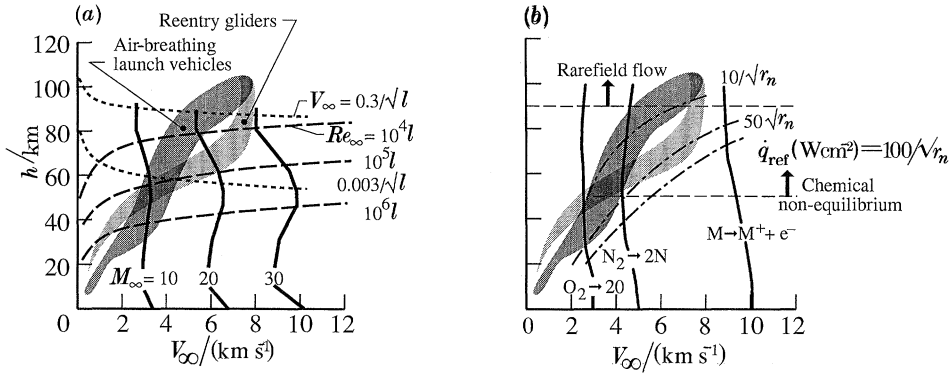

Figure 1. Vehicle flight domains with contours of constant Mach number, M_∞, Reynolds number, Re_∞, viscous interaction parameter, $\bar{V}'_\infty$, and stagnation point heating rate, $\dot{q}_s$, and boundaries for dissociation, ionization, chemical non-equilibrium and rarefied flow.

occur when $\bar{V}'_\infty > 0.1$, figure 1 shows that such effects will be important only during the very early portions of the entry trajectory. Turning to figure 1*b*, it is seen that these vehicles will experience significant dissociation and chemical non-equilibrium effects and high levels of convective heating. Conversely, rarefied flow effects will be of secondary importance, occurring only at very high altitudes.

(*b*) *Air-breathing launch vehicles*

Air-breathing launch vehicles and re-entry gliders fly through the same range of Mach numbers. However, because of the large size of the air breathers (Sanger is 85 m long) and the different shape of their flight corridor, they experience smaller viscous interaction effects and significantly higher Reynolds numbers. Furthermore, the regions of highest aerodynamic heating and loads occur at altitudes between 20 and 40 km rather than between 50 and 80 km as was the case for re-entry gliders. Because they use atmospheric oxygen instead of on-board oxidizers, air breathers tend to fly a high dynamic pressure (low altitude) ascent trajectory until aerodynamic heating levels become excessive. Then they pull up and fly a more ballistic type of trajectory to reduce heating levels. If the same criteria for turbulent flow and viscous interaction effects are assumed, it is seen that airbreathers will experience turbulence during their low-altitude ascent including the peak heating regions. Then, following the pull-up, their boundary layers would be expected to return to a laminar state. Viscous interaction and rarefied flow effects should be of secondary importance.

Figure 1*b* shows that while significant oxygen dissociation may occur, nitrogen dissociation will be negligible during the high-heating, non-ballistic portion of the flight domain. For vehicles flying near the upper boundary of the flight domain (typical of Sanger and HOTOL), oxygen dissociation and subsequent chemical relaxation (non-equilibrium) effects should have little influence on external flows. For vehicles flying near the lower bound (typical of vehicles which utilize air-breathing propulsion to higher Mach numbers), dissociation and chemical non-equilibrium could be important. One important exception to the above statements about non-equilibrium should be noted. Chemical relaxation of the hot, dissociated engine exhaust products as they expand over the nozzle surfaces can have a first-order effect on air-breather performance. Since there are no pertinent flight data, the present paper does not address exhaust or inlet flows.

PHILOSOPHICAL TRANSACTIONS OF THE ROYAL SOCIETY A MATHEMATICAL, PHYSICAL & ENGINEERING SCIENCES

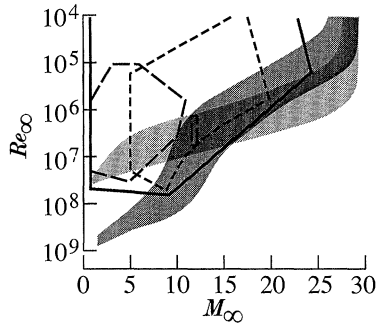

Figure 2. $M_\infty - Re_\infty$ capabilities of ground-based test facilities compared to vehicle flight domains. Envelope of currently available facilities (——), low-temperature tunnels used in Shuttle programme (——), and shock tunnels used in Shuttle programme (– – –).

4. Ground test capability

In figure 2, the Mach number/Reynolds number capabilities of ground based test facilities are presented and compared with the previously discussed flight domains. The solid line is the envelope of currently available facilities. The dashed lines indicate the capabilities of conventional low-temperature wind tunnels and shock tunnels used in the Shuttle programme. It should be noted that our ground test capability has increased relatively little since the Shuttle tests were carried out.

It is seen that, through the use of both conventional, perfect-gas wind tunnels and impulse facilities (shock tunnels, etc.), Mach number/Reynolds number simulation is possible over a significant portion of the re-entry glider flight domain and for air-breathing launch vehicles flying near the low Reynolds number bound of their flight domain. As mentioned earlier, Sanger and HOTOL operate in this region. The fact that overall aerodynamic characteristics tend to be only weakly dependent on Mach number for $M > 8$ makes the limited Mach number capability of conventional wind tunnels relatively unimportant so long as flow chemistry effects are absent. When significant dissociation and chemical relaxation occurs, however, ground based facilities have an inherent scaling problem that cannot be overcome. Impulse facilities and arc-heated wind tunnels can be operated at high enough enthalpies to produce realistic post-shock temperatures and hence dissociation levels. However, the ensuing chemical reactions (e.g. atom recombination) have characteristic time constants determined by local densities and temperature. Since the velocity fields will be comparable in flight and in an accurate ground simulation, a fluid element that undergoes a given chemical reaction (e.g. percent recombination) will, in doing so, travel approximately the same distance in the ground test as in flight. Hence, this reaction might occur near the nose of a 33 m long Shuttle but would not occur until a point is reached that is well downstream of a 0.01 scale (0.33 m long) wind tunnel model. Hence, the composition of the gas in the model's flow field may be quite different from that for the flight vehicle. As is shown in figure 1*b*, however, there are large portions of the re-entry glider and air-breathing launch vehicle flight domain where flow chemistry is relatively unimportant. Flight data can be used to identify those vehicles and flight régimes for which wind-tunnel test results can be confidently extrapolated to flight conditions.

PHILOSOPHICAL TRANSACTIONS OF THE ROYAL SOCIETY A MATHEMATICAL, PHYSICAL & ENGINEERING SCIENCES

5. Computational capability

With the enormous advances in digital computing capability that have occurred in recent years, it is now possible, in principle, to accurately predict the distributions of pressure and aerodynamic heating over complex geometries at hypersonic flight conditions with high temperature, chemically reacting flow fields. In practice, however, there are still practical limits on computer speed and storage. In fact, most present day Navier–Stokes solutions are limited to perfect gases. While Navier–Stokes solutions with finite-rate chemistry and complex geometries are available, they can take days to compute a single velocity–altitude flight condition. Hence, it is important to know when simplifying assumptions like equilibrium chemistry or perfect gas can be used and flight test data can be extremely helpful in this regard.

6. Flight test programmes

In the present paper, five flight test programmes are reviewed. They are the X-15 programme, Asset and Prime, Reentry F and the Space Shuttle Orbiter. These programmes and their flight dates are presented in table 1.

The configurations of the flight vehicles and typical trajectories are presented in figures 3 and 4 respectively. Of these five programmes, all were re-entry flight tests except for the X-15 which was airlaunched from a B52 carrier aircraft, and flew a rocket powered, lifting ascent trajectory followed by a gliding re-entry into the lower atmosphere. Hence, the X-15 flight domain comes closest to that of the air-breathing launch vehicles. The Space Shuttle Orbiter, of course, produced the definitive set of flight data for re-entry gliders. The Asset and Prime programmes provided early flight experience in the re-entry glider flight domain. While most of the Asset and Prime flight data are still classified or restricted and hence not available in the open literature, certain overall results have been made public and tend to complement the Shuttle data.

Fascinating historical reviews of the X-15, Asset and Prime programmes have been presented by Hallion (1983, 1987) and Powell & Hengeveld (1983). The Reentry F programme was flown to obtain flight data on transition and turbulent heating at high hypersonic Mach numbers. The resulting data is of interest in studies of air-breathing launch vehicles even though the boundary layer over most air-breathers should have relaminarized by the time they reach $M = 20$.

X-15

The X-15 programme spanned 15 years, with three aircraft carrying out a total of 199 flights. The flight vehicles were heavily instrumented (295 thermocouples, 136 pressure orifices) and produced a large, definitive body of flight data at Mach numbers up to 6.7. Highlights of the programme have been reviewed by Becker (1969). Representative aerodynamic and heating data have been presented by Pyle (1964, 1965), Keener & Pembo (1962) and Banner *et al.* (1962).

Perhaps the greatest contribution of the X-15, from the viewpoint of the present paper, was to conclusively demonstrate that there was no hypersonic 'facilities barrier' so long as flight velocities are not high enough to produce significant dissociation. As pointed out by Becker (1969), many aerodynamicists of that era expected that because of strongly interacting flow fields, viscous interactions with

PHILOSOPHICAL TRANSACTIONS OF THE ROYAL SOCIETY A MATHEMATICAL, PHYSICAL & ENGINEERING SCIENCES

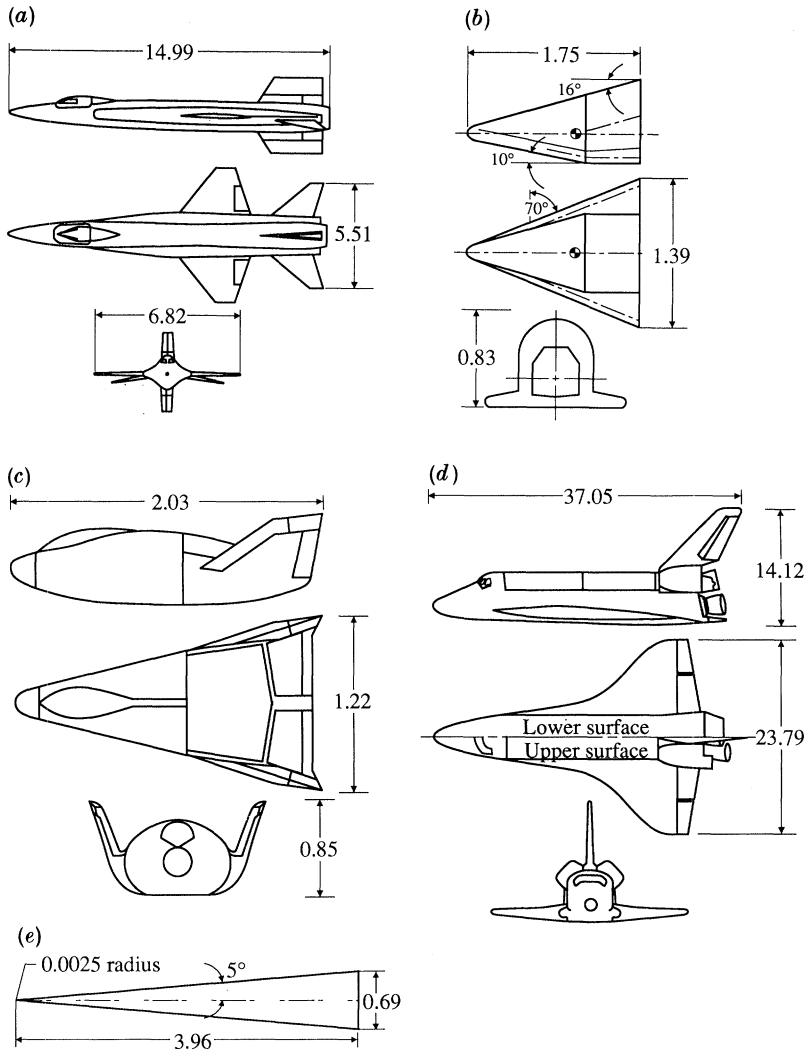

Figure 3. Flight test vehicles: (*a*) X-15, (*b*) Asset, (*c*) Prime, (*d*) Shuttle, (*e*) Reentry F. All dimensions in metres.

Table 1. *Hypersonic flight test programmes*

type	date
X-15	17 September 1959–15 November 1967
Asset	18 September 1963–23 February 1965
Prime	21 December 1966–5 March 1967
Reentry F	1968
Shuttle (OFT)	April 1981–December 1982

strong shocks and possible real-gas effects, the X-15 would reveal large discrepancies between wind tunnel data and flight. To the contrary, X-15 data showed that virtually all the flight results were in excellent agreement with low-temperature, perfect-gas wind tunnel predictions.

PHILOSOPHICAL TRANSACTIONS OF THE ROYAL SOCIETY A MATHEMATICAL, PHYSICAL & ENGINEERING SCIENCES

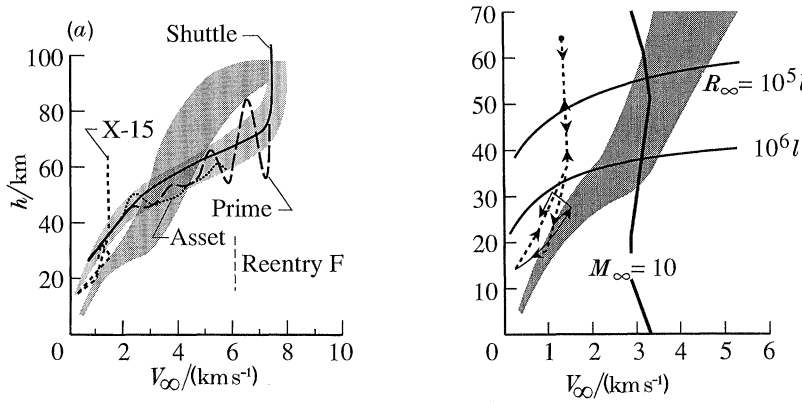

Figure 4. Flight test trajectories compared to vehicle flight domains. (*a*) Typical trajectories for X-15, Asset, Prime, Reentry F and Shuttle Orbiter, (*b*) high altitude (– – –) and low altitude (——) trajectories for X-15.

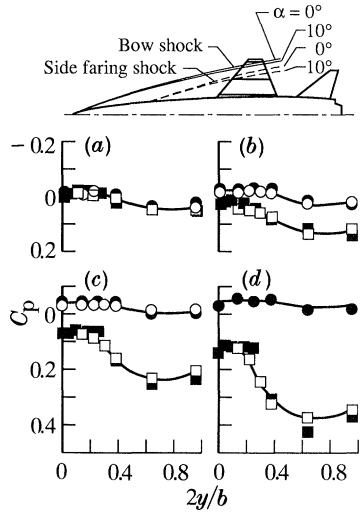

Figure 5. Upper (○, ●) and lower surface (□, ■) spanwise pressure coefficient distributions: (*a*) $\alpha = 0°$, (*b*) $\alpha = 5°$, (*c*) $\alpha = 10°$, (*d*) $\alpha = 15°$. Comparison of flight data with (○, □, ——) wind tunnel data (●, ■) (Pyle 1965).

A typical example of this agreement is presented in figure 5 where it is seen that wind tunnel and flight pressure data agree quite well even though there are strong interactions between the bow and side-fairing shocks and the wing flow field. As would be expected, the X-15 data also exhibited excellent agreement between ground-test and flight for integrated aerodynamic coefficients and stability derivatives.

Figure 6 shows a typical set of data for the longitudinal and directional control derivatives. As Becker also points out, the period between the conception and completion of the X-15 programme was a time of intensive research on high-temperature, real-gas flows. In the early 1950s it was thought that wind tunnels with stagnation temperature levels comparable with flight (e.g. arc-heated tunnels) would be required to accurately predict vehicle characteristics in the X-15 flight régime. By the mid 1960s it was clear that significant real-gas effects would not occur at

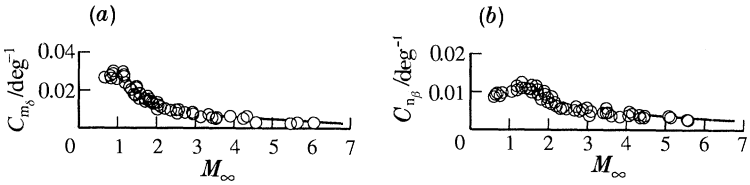

Figure 6. Longitudinal (*a*) and directional (*b*) control derivatives for the X-15. Comparison of flight data (○) with faired wind tunnel data (——) at $\alpha = 4°$ (Becker 1969).

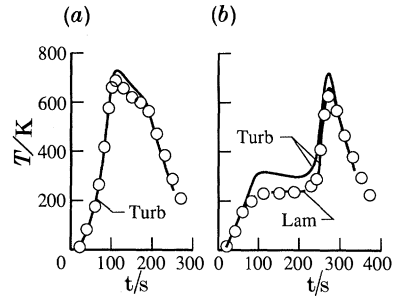

Figure 7. X-15 wing skin temperatures. (*a*) low altitude trajectory, (*b*) high altitude trajectory. Turbulent and laminar predictions (——) compared with flight data (○) (Banner *et al.* 1962).

Mach numbers below approximately 10 (i.e. below the onset of dissociation, see §3) and that low stagnation temperature, perfect-gas wind tunnel data would have wider applicability than had been thought. The X-15 showed conclusively that this was true.

The X-15 also produced significant aerodynamic heating data. In figure 7 typical low- and high-altitude flight results are presented for a point on the wing lower surface at mid semi-span and 0.43 m downstream of the leading edge. Corresponding low-altitude and high-altitude trajectories for the X-15 are shown in figure 4*b*.

It is seen that the low-altitude trajectory produced Reynolds numbers (based on the X-15s length of 15 m) greater than 10^7. Hence, turbulent boundary layers would be expected. On the other hand, the high-altitude trajectory traverses a Reynolds number range from greater than 10^7 to *ca.* 3×10^5 and then back to greater than 10^7. Hence, for the high-altitude trajectory, the boundary layer would be expected to start out turbulent, change to laminar during the X-15s climb to maximum altitude and then undergo transition back to turbulent as the X-15 re-entered the dense lower atmosphere. Figure 7 shows this behaviour and also shows that, with exception of an over-prediction near peak (turbulent) heating, flat plate boundary-layer theory (*ca.* 1962) did a good job of predicting both laminar and turbulent heating rates over the wing. The phenomenon of 'relaminarization' illustrated by the high-altitude trajectory results in figure 7 is of significance for airbreathing launch vehicles which are likely to experience turbulent heating followed by relaminarization at some point during ascent. The occurrence of relaminarization and the time when it occurs have a major effect on the integrated heat load that the vehicle structure must be designed to withstand. It would be expected that relaminarization would occur near the critical Reynolds number (i.e. a neutrally stable state for the boundary layer) whereas transition to turbulence usually occurs at Reynolds numbers considerably larger than the critical value. If the data presented in figure 7 are interpreted as indicating relaminarization at 65 s and subsequent transitions to turbulence at

240 s, the corresponding free-stream Reynolds numbers (based on vehicle length) are approximately 9×10^5 at relaminarization and 4×10^6 at transition. These numerical values should not be used to predict the boundary layer state on future vehicles for two reasons. First, a criterion based on local flow conditions is much to be preferred over free stream Reynolds number as an indicator of boundary layer state. Secondly, transition on the X-15 appeared to be influenced strongly by large wing-leading-edge expansion joints which were configuration specific. The data shown on figure 7 do, however, suggest that the criterion for relaminarization may differ significantly from that for transition to turbulence.

(*b*) *Asset and Prime*

Asset and Prime were small, lifting vehicles that provided early hypersonic flight experience in the re-entry glider flight domain. Asset was a highly swept delta wing configuration, whereas Prime was a lifting body. The primary purpose of the Asset programme was to obtain aerothermodynamic and materials response data under hypersonic flight conditions. The Asset vehicles were covered with high-temperature metallic heat shields (with the exception of the wing leading edges which were graphite and the nose cap which was thoria-tungsten or zirconia depending on the vehicle) and were well instrumented with surface thermocouples and pressure orifices. The quantitative data from both programmes remain classified or restricted. Qualitative results are, however, available along with fairly detailed descriptions of the programmes, vehicles and trajectories (Powell & Hengeveld 1983; Hallion 1987). From an aerothermodynamic stand point, both programmes produced impressive verifications of hypersonic-vehicle design techniques. In fact the only reported major disagreement was the underprediction of hypersonic trim angle-of-attack for the Asset vehicle. As we shall see, this is a recurrent problem for hypersonic vehicles. Table 2 contains information about the successful flights in the two programmes. Trajectories for the Asset flights are presented in figure 8 and a nominal high cross-range design trajectory and predicted stagnation point heating rates for Prime are presented in figure 9.

As shown in figure 9, initial conditions for the Prime flights corresponded to entry from low Earth orbit. The vehicle was controllable in both pitch and roll through the use of lower-surface, trailing-edge flaps and reaction control jets located on the base. It appears, however, that active pitch modulation was not used and flights were characterized by a pronounced re-entry phugoid oscillation (see figure 9) and flight at high bank angles (39°–46°) to produce cross-range. From all indications, the vehicle's aerothermodynamic performance was essentially as predicted by perfect-gas wind tunnel data extrapolated to flight conditions. Those small discrepancies that were encountered were attributed to ablation effects, but ablation of the heatshield was not great enough to produce significant degradation in stability and control, and the vehicles responded well to flap commands (Hallion 1987). The accuracies with which the Prime vehicles were guided to their targets are truly impressive, especially in view of the fact that the ground based terminal guidance was inoperative for FV-3.

While the maximum velocities reached in the Asset programme were sub-orbital (see figure 8) they were high enough to produce relatively high levels of aerodynamic heating and potentially significant real-gas effects (see figures 1*b* and 4).

As shown in figure 8, all the vehicles except ASV-4 followed relatively smooth equilibrium-glide trajectories. ASV-4 experienced a phugoid oscillation early in its

PHILOSOPHICAL TRANSACTIONS OF THE ROYAL SOCIETY A MATHEMATICAL, PHYSICAL & ENGINEERING SCIENCES

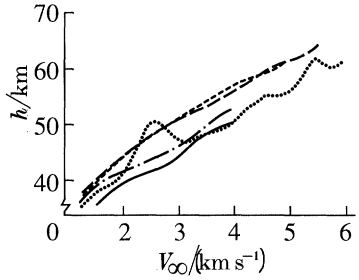

Figure 8. Asset trajectories for vehicles ASV-1 (– – –), ASV-3 (——), ASV-4 (· · · · ·), AEV-1 (——) and AEV-2 (—·—) (Hallion 1987).

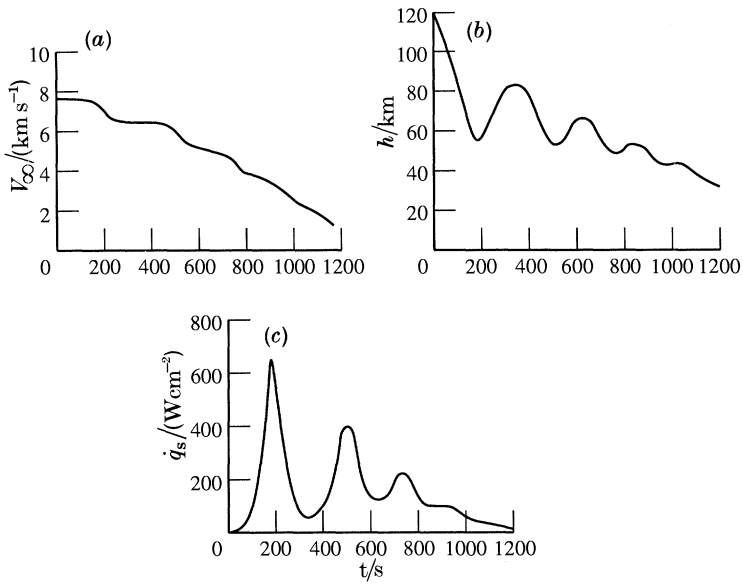

Figure 9. Predicted entry time histories for Prime high cross-range mission. (*a*) velocity, (*b*) altitude, and (*c*) stagnation point heating rate (Hallion 1987).

entry which damped out as altitude decreased. The pull-up manœuver between 3 and 1.8 km^{-1} s was accomplished by means of a mercury-transfer ballast system which shifted the centre of gravity. Two types of vehicles were flown in the Asset programme. Those designated ASV in table 2 were 'aerothermodynamic structural vehicles' intended to produce data on the distributions of pressure and aerodynamic heating and or the response of various thermal-protection-system concepts to the hypersonic environment. The surface materials (and their maximum design temperatures) included: refractory columbium (1756 K), a cobalt-based alloy called L-605 (1367 K), TZM molybdenum (1922 K), graphite leading edges (1922 K), and thoria-tungsten or zirconia nose caps (2478 K). The ASV vehicles telemetered data from 104 engineering parameters (59 temperatures, 35 pressures, 6 deflections and 4 accelerations) to the ground. The vehicles designated AEV were 'aerothermoelastic vehicles.' Their primary experiments were a 0.3 m by 0.6 m flap located on the rear bottom surface to evaluate unsteady aerodynamic effects on control surfaces, and a corrugated columbium panel (located ahead of the flap) to investigate aeroelastic panel flutter.

Table 2. *Asset and Prime flights*

date	vehicle designation	h_i/km	V_i (kms^{-1})	α_{trim}/deg	range/km (cross-range)	dispersion/km
18/09/63	Asset ASV-1	61.9	4.91	38	1228 (0)	97 uprange
22/07/64	Asset ASV-3	64.6	5.5	38	2655 (0)	—
27/10/64	Asset AEV-1	50.4	3.97	20	1448 (0)	*ca.* 72 uprange
08/12/64	Asset AEV-2	52.9	3.97	26	1370 (0)	*ca.* 68 uprange
23/02/65	Asset AEV-4	61.6	5.91	20	4344 (0)	151 uprange
21/12/66	Prime FV-1	122	7.71	*ca.* 35	8000[a] (0)	0.3
05/03/67	Prime FV-2	122[a]	7.9[a]	*ca.* 35	8000[a] (1052)	3.5
19/04/67	Prime FV-3	122	8.17	*ca.* 35	8000[a] (1482)	7.9

[a] Nominal mission values.

The flight data showed excellent agreement with prediction with the exception of hypersonic trim angle-of-attack which increased with increasing Mach number whereas wind tunnel data predicted the reverse. On ASV-4 which flew at the highest velocities the trim angle-of-attack was 25° as compared with the predicted value of 20° (Hallion 1987).

The result of this angle-of-attack underestimation was a lower L/D, which led to an error of approximately 5% in predicted range. As shown in table 2, this plagued the entire programme. From an aerothermodynamic standpoint, a likely cause is that hypersonic flight pitching moments are significant different from wind tunnel values because of real-gas effects. Such an explanation becomes more believable when the Shuttle flight data, which exhibit exactly this behaviour, are examined.

Reentry F

Over the years, a sizable flight data base on aerodynamic heating for conical vehicles has accumulated, largely as part of various ballistic-missile re-entry vehicle programmes. On many of these vehicles, instrumentation was limited to that needed to assess vehicle performance and accuracy. On others, ablation effects and configuration peculiarities prevent straight forward interpretation and generalization of the results. None the less, the overall quantity of flight data is large and has been reviewed and assessed by several researchers (Beckwith & Bertram 1972; Berkowitz *et al.* 1977). Reentry F was flown to produce a benchmark set of flight turbulent heating data at high local Mach numbers. The vehicle was carefully instrumented and the resulting flight data was meticulously reduced and analysed (Wright & Zoby 1977). The resulting data-set complements the large body or re-entry vehicle data and is useful for assessing aerodynamic theories since, because of the sharp-cone flowfield, boundary-layer edge conditions are well known. Comparisons between modern rigorous heating predictions and the Reentry F data have shown excellent agreement (Sutton *et al.* 1988). An example of such agreement is presented in figure 10.

PHILOSOPHICAL TRANSACTIONS OF THE ROYAL SOCIETY A MATHEMATICAL, PHYSICAL & ENGINEERING SCIENCES

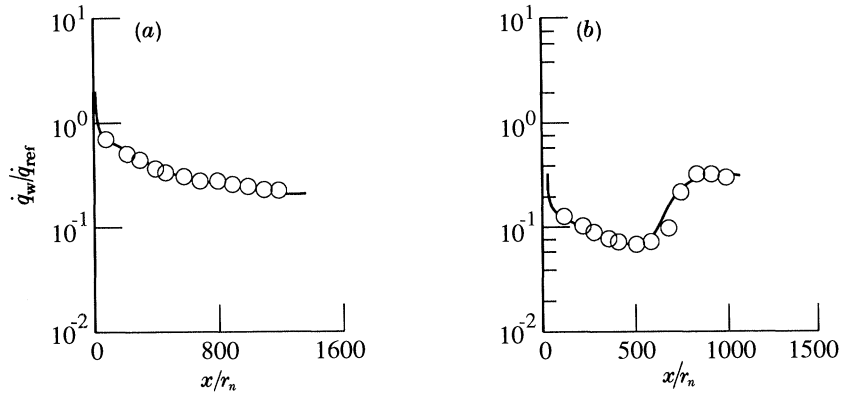

Figure 10. Heating rate distributions for Reentry F. (*a*) $h = 36.6$ km, $M_\infty = 19.25$, $\alpha = 0°$. (*b*) $h = 24.4$ km, $M_\infty = 19.97$, $\alpha = 0.14°$ leeward ray. Comparison of viscous shock layer predictions (——) with flight data (○) (Sutton *et al.* 1988).

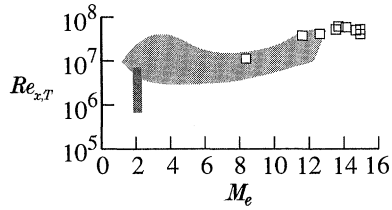

Figure 11. Flight data on boundary layer transition. Reentry F results (□) compared with the envelop of data for 2.5° to 30° half-angle cones (light shading) and to Shuttle data (dark shading) (Wright & Zoby 1977; Goodrich *et al.* 1983; Stetson 1987).

It should be noted that the good agreement shown in figure 10 for transitional heating is the result of judicious *a posteriori* modelling (i.e. beginning and end of transitional region, etc.). Prediction of transitional heating is beyond the current state-of-the-art. It has also been shown (Sutton *et al.* 1988) that flat-plate boundary-layer theory can yield accurate predictions of the Reentry F flight results when it is applied with careful evaluation of edge conditions and temperature dependent gas properties, and the use of the Mangler transformation to account for conical flow. Another goal of the Reentry F project was to provide flight data on boundary-layer transition at high local Mach number. In figure 11, the Reentry F transition results are presented along with other available flight data. The high Mach number Reentry F data, when considered together with the other data in figure 11, indicate a trend of increasing boundary-layer-edge transition Reynolds number with edge Mach numbers. However, the range of transition Reynolds numbers shown in figure 11 indicates our present inability to predict transition to within better than an order of magnitude. This will be discussed further in the context of the Shuttle data.

(*d*) *Shuttle Orbiter*

The first five flights of the Space Shuttle, designated OFT-1 (for Orbiter flight test 1) to OFT-5, provided a wealth of data on a wide range of phenomena of importance to re-entry gliders and airbreathing launch vehicles. For these five flights, the Space Shuttle *Columbia* was equipped with an instrumentation system comprised of over 4500 sensors, associated data-handling electronics and a recorder.

Included in the instrumentation were extensive surface pressure and temperature measurements, special instrumentation to assess the response of the thermal protection system tiles, and an aerodynamic coefficient identification package (ACIP) which enabled the extraction of aerodynamic stability derivatives. Following these OFT flights, two comprehensive conferences were held to review the results. The proceedings were published as NASA conference publications (Arrington & Jones 1983; Chaffee 1985) and provide comprehensive presentations and analyses of the flight data. These flight test results have also been addressed in numerous technical journal articles (most notably in the AIAA *J. Spacecraft Rockets*) and were compared with computational fluid dynamic analyses by Sutton *et al.* (1988). Selected results from these Shuttle flights are presented in figures 12–23 and are discussed in the following sections of this paper.

(i) *Aerodynamics*

Prediction of the Shuttle Orbiter aerodynamic characteristics was based on an extensive programme of wind tunnel tests. By the first Shuttle flight, approximately 46000 hours of wind tunnel tests had been carried out consisting of 24900 hours for the orbiter, 17200 hours for the mated launch configuration and 3900 hours for the carrier aircraft program. A total of 101 models were built: 45 aerodynamic, 34 heat transfer, and 22 structural dynamic (Whitnah & Hillje 1982). Aeroelastic effects on longitudinal stability were accounted for analytically. Lateral directional stability and rudder effectiveness were assessed using wind tunnel models with flexible tails (Schlosser & Dominik 1983). The resulting data formed the basis for the Aerodynamic Design Data Book (Rockwell International Space Division 1980). This data book contained not only the basic wind tunnel data but also 'variations' which were estimates of the amount by which actual flight results could differ from the data book values. These variations accounted for experimental inaccuracies, test-to-test repeatability and wind-tunnel-to-flight-test differences experienced in past aircraft programmes (Young & Underwood 1983). Predictions from the data book along with the associated variations represent the state-of-the-art in hypersonic aerodynamics *ca.* 1977. Shuttle flight results that fall outside the data book variations suggest incompletely understood phenomena.

The similarity parameters used to correlate and extrapolate the wind tunnel results to flight conditions were Reynolds number, Mach number and the viscous interaction parameter,

$$\bar{V}'_\infty = M_\infty \sqrt{(C'_\infty / Re_\infty)}, \tag{1}$$

where C' is the proportionality factor in the linear viscosity–temperature relation, i.e.

$$C'_\infty = \rho' \mu' / \rho_\infty \mu_\infty \tag{2}$$

and ρ' and μ' are evaluated at the reference temperature,

$$T'/T_\infty = 0.468 + 0.532 T_w/T_\infty + 0.195 \tfrac{1}{2}(\gamma - 1) M^2_\infty. \tag{3}$$

For Mach numbers from approximately 4 to 13, wind tunnels were capable of near-flight Reynolds numbers (Romere & Young 1983) and hence (excluding real-gas effects), no corrections were required. At lower Mach numbers, the traditional adjustments were applied for Reynolds number effect on skin friction drag. At higher Mach numbers (above approximately 15) $\bar{V}'_\infty$ was used as the primary scaling parameter. It should be noted that viscous interaction effects were predicted to be

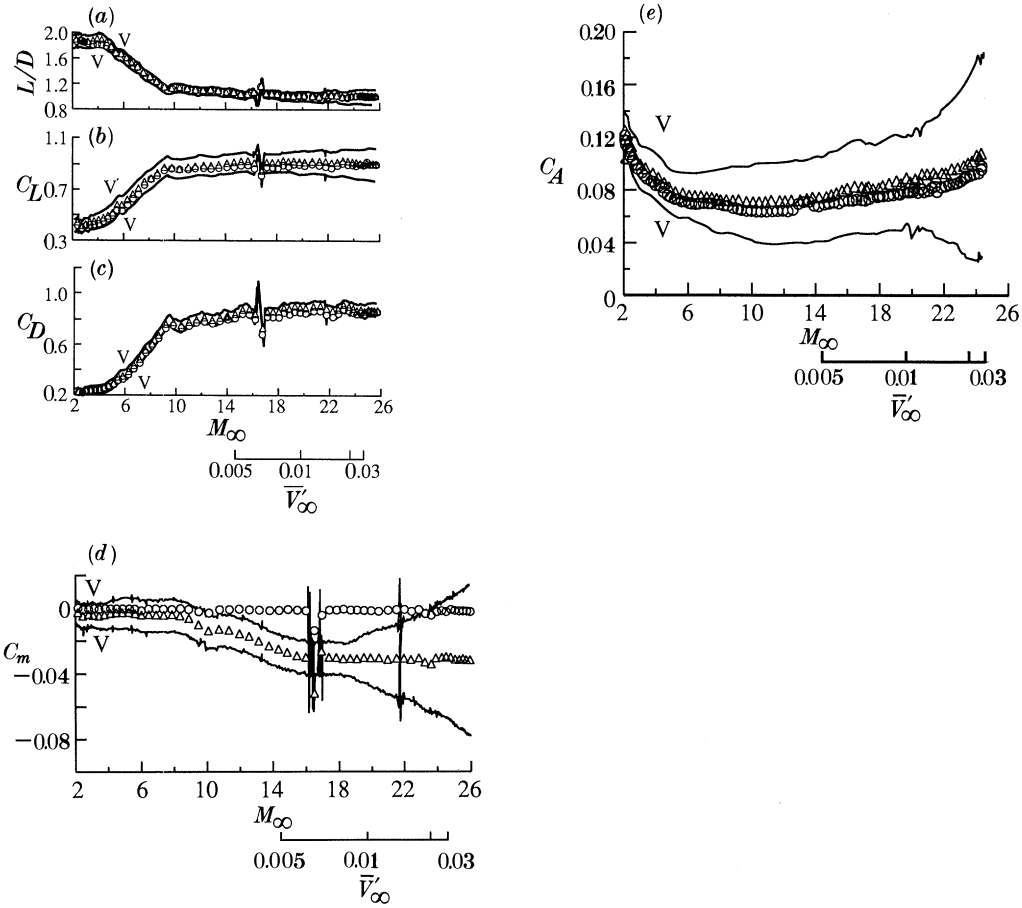

Figure 12. Shuttle aerodynamic characteristics. (*a*) lift-to-drag ratio (STS-5), (*b*) lift coefficient (STS-5), (*c*) drag coefficient (STS-5), (*d*) pitching moment coefficient (STS-5), and (*e*) axial force coefficient (STS-2). Comparison of flight data (○) with data book predictions (△) and variations (V) (Compton *et al.* 1983; Romere & Young 1983).

significant for axial force and to be small-to-negligible for normal force and pitching moment (Woods *et al.* 1983). Real-gas effects were judged to fall within the scatter of the wind tunnel data base and were assumed to be accounted for by the previously mentioned variations.

As shown in figure 12, the methodology described above produced accurate predictions of lift and drag coefficient and lift-to-drag ratio throughout the supersonic and hypersonic flight régimes. The results shown in figure 12*a–e* are for STS-5 but the agreement is typical of that obtained on all five OFT flights (Compton *et al.* 1983; Romere *et al.* 1983; Romere & Young 1983). Not only do the flight data points fall within the variation bounds, they are also quite close to the predicted values. The apparent under-prediction of C_L and C_D in the $M = 10$–27 range has subsequently been shown to be due to an inaccurate definition of atmospheric density. When the density is corrected, the true agreement approaches that shown for L/D. As shown in figure 12*e* an increase in axial force coefficient is seen for $\bar{V}'_\infty \gtrsim 0.005$ ($M_\infty > 12$). Hence, the $\bar{V}'_\infty$ correlation appears to have been successful in accounting for viscous interaction effects.

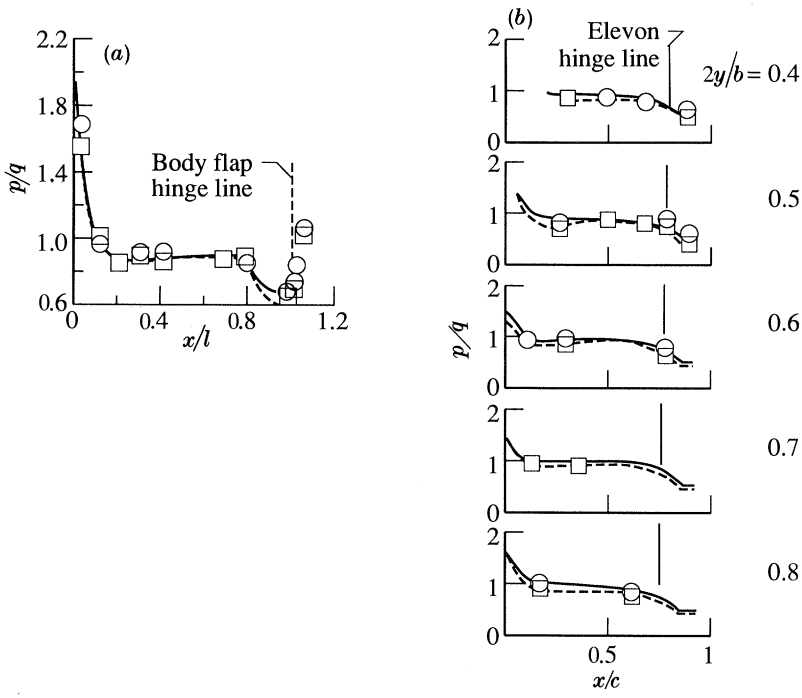

Figure 13. Shuttle windward surface pressures. (*a*) fuselage centreline, and (*b*) wing. Comparison of flight data from STS-3 (○) and -5 (□) with Euler code predictions for $\gamma = 1.4$ (——) and $\gamma_{\text{eff}} = 1.18$ (– – –) (Sutton *et al.* 1988).

The predicted pitching moments did not, however, agree with flight results. A typical comparison is shown in figure 12*d*. Since the flight vehicle was trimmed, pitching moment was zero throughout the entry. However, the body flap deflections δ_{bf}, required to trim the orbiter at the desired angle-of-attack were considerably larger than had been predicted. For example, on STS-1 the δ_{bf} required to trim the vehicle at $M_\infty > 20$ was approximately 16° (downward) as opposed to the nominal predicted value of 8° (Woods *et al.* 1983). When the flight values of V_∞, h, α and δ_{bf} are used with the aero data book, the resulting predicted pitching moments are as shown by the triangles in figure 12*d*. It appears that, in flight at $M_\infty > 18$, the orbiter experienced an unexpected nose-up pitching moment increment of approximately 0.03 hence requiring an additional body flap deflection of 8° for trim. Note that the predicted values begin to deviate from the flight values at a Mach number of approximately 8, which corresponds roughly to the onset of dissociation as shown in figure 1*b*. This suggests a real-gas effect. In fact, based on analyses carried out by Hamilton & Weilmuenster (Sutton *et al.* 1988) and Maus *et al.* (1984) this is the case.

Hamilton & Weilmuenster computed pressure distributions over the windward surface of the orbiter at angles-of-attack up to 40° by means of an explicit, three-dimensional, time-asymptotic Euler code called HALIS (Weilmuenster & Hamilton 1983). Their results are presented for the fuselage windward centreline in figure 13*a* and for five spanwise locations on the wing in figure 13*b*. In both figures, flight data are compared with perfect-gas calculations for $\gamma = 1.4$, which corresponds to wind tunnel conditions and for $\gamma = 1.18$ which is an 'effective γ' that results in the same shock density ratio as equilibrium air and is believed to approximate flight

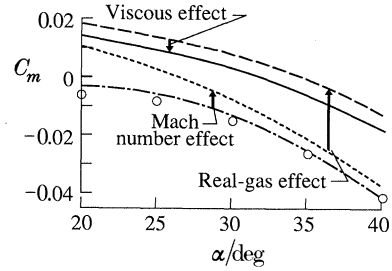

Figure 14. Shuttle pitching moment. Use of CFD predicted real-gas effects to extrapolate $M = 8$ wind tunnel data (—·—) to hypersonic flight conditions ($M_\infty = 23$, $h = 73.1$ km, $\delta_e = \delta_{bf} = 0°$ (——). Circles are data book predictions for $M_\infty = 20$, $\delta_e = \delta_{bf} = 0$ (Maus *et al.* 1984).

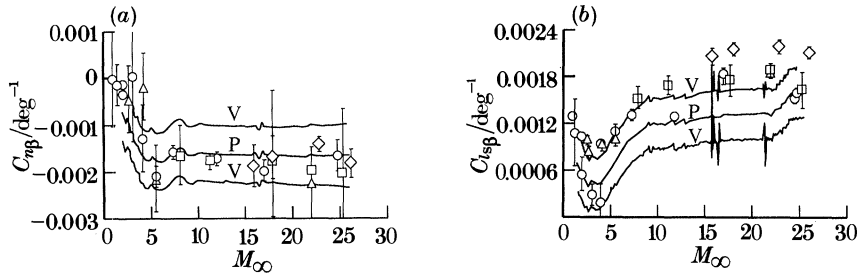

Figure 15. Shuttle control derivatives. (*a*) Yawing moment due to sideslip, (*b*) rolling moment due to aileron. Flight data for STS-2 (○), -3 (□), -4, (◇), and -5 (△) with Cramer–Rao bounds (I) compared to data book predictions (P) and variations (V) (Compton *et al.* 1983).

conditions. Note that the $\gamma = 1.18$ calculations yield lower pressures over the aft portion of the fuselage and over much of the wing and are in better agreement with the flight data. The magnitudes of the pressure differences are small but they act over a large area. The entire wing surface outboard of $2y/b = 0.5$ lies aft of the vehicle centre of gravity. Hence, it is believable that the integrated effect would be a sizable nose-up pitching moment. Maus *et al.* (1984) carried out a similar analysis using different CFD techniques. They used a modified orbiter geometry to facilitate computations at high angles of attack and showed by comparison with wind tunnel data that the modified geometry was a good aerodynamic approximation of the Space Shuttle. They then carried out equilibrium-air inviscid flow field calculations to assess Mach number and real-gas effects. The results of these calculations were then used to extrapolate $M = 8$ wind tunnel data to flight conditions. The results are shown in figure 14 for a $M = 23$ flight condition. Note that at $\alpha = 40°$, real-gas effects produce a nose-up pitching moment increment of approximately 0.03 which largely accounts for the discrepancy between flight data and predictions. It has also been shown by Maus *et al.* (1984) and by Romere & Young (1983) that the orbiter body flap and aileron effectiveness in flight was well predicted by data book values. Hence, it appears that the hypersonic trim discrepancy was due to an error in predicting the basic vehicle pitching moment caused by real-gas effects that can not be simulated in conventional air wind tunnels.

In retrospect, it seems highly likely that the hypersonic trim anomaly that plagued the Asset programme was due to similar real-gas effects.

Stability and control derivatives were usually well within the data book variations. Typical results are shown for yawing moment due to sideslip and rolling moment due to aileron in figure 15*a*, *b* respectively. The estimated derivatives were obtained

using the modified maximum likelihood estimation method (MMLE-3) developed by Maine & Iliff (1980). The Cramer–Rao bounds are measures of the accuracy of the estimation process. The true Cramer–Rao bounds represent a lower limit on the variance of the estimated parameters. A factor of 10 was generally accepted as a conservative multiplicative factor for association with Shuttle results. As shown in figure 15, the agreement at hypersonic Mach numbers is generally good though large Cramer–Rao bounds for some points indicate possible uncertainties associated with the estimation process (Compton *et al.* 1983).

Aside from the previously discussed longitudinal trim anomaly, the largest aerodynamic discrepancies were observed for the effectiveness of the reaction control system (RCS) jets which were located at the base of the OMS (orbital manoeuvering system) pods on either side of the vertical tail. At high altitudes (hence low dynamic pressure) a blended control system composed of aerodynamic surfaces plus reaction control jets must be used to provide adequate control authority. Also, because of low rudder effectiveness the yaw jets were used at Mach numbers down to 1.0.

The generation of the RCS data base required the development of simulation parameters to correlate the wind tunnel test data. A number of parameters suggested in the literature were investigated, and it was determined that jet mass flow ratio, based on one side-jet firing, best correlated the yaw-jet data and that jet momentum ratio, based on the total number of jets firing, best correlated pitch-jets data. Hence these simulation parameters were used in developing the aero data book. However, it was recognized that because of strong interactions between the jet plumes and the orbiter flow field, especially in case of the yaw jets, adequate simulation was probably impossible in conventional wind tunnels (Kanipe 1983; Stone & Baumach 1983).

Results from the Shuttle flights showed a number of discrepancies between flight results and data book predictions. At high altitudes, the effectiveness of the pitch jets was less than predicted. This was attributed to the inability of available tunnels to duplicate the low pressures characteristic of the high altitude wake flow. The yaw jets were more effective than predicted in producing side force and yawing moment and were significantly less effective than predicted in producing rolling moment at high Mach numbers. Results for the yaw jets are presented in figure 16.

It has been shown that the difference between flight and data book values for the increment in rolling-moment coefficient due to yaw jet firing is attributable to interactions between the jet plume and the flow over the orbiter wing (Compton *et al.* 1983). The underprediction of the increment in side-force coefficient appears to be due to an inability to match the appropriate local Reynolds number and hence the flow separation location in the tunnel tests. On STS-1, early in the entry, a large oscillation occurred in sideslip. This behaviour was attributed to the underprediction of roll due to yaw jet firing shown in figure 16*a*. Since re-entry gliders must use blended control systems at high altitudes, RCS jet interaction effects can be important. At present, however, adequate wind tunnel simulation does not appear possible and numerical simulation of the geometrically complex, viscous dominated, jet interaction flow fields would be a challenging CFD task.

While the Orbiter's entry performance is only slightly influenced by rarefied flow effects, they are of considerable fundamental interest. Also, the vehicles' rarefied flow aerodynamic characteristics are important in determining its response to a blended control system. As part of the NASA Orbiter Experiments Programme, the Orbiter *Columbia* was equipped with a high resolution accelerometer package (HIRAP) which

PHILOSOPHICAL TRANSACTIONS OF THE ROYAL SOCIETY A MATHEMATICAL, PHYSICAL & ENGINEERING SCIENCES

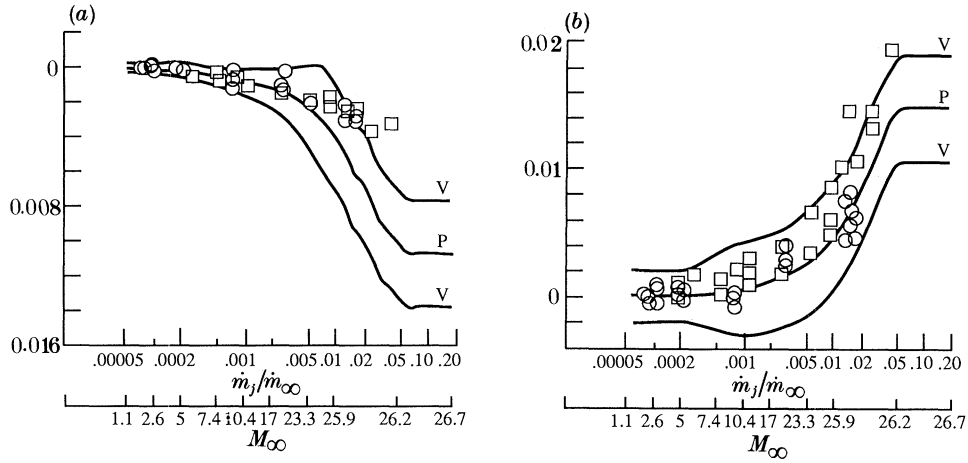

Figure 16. Shuttle control moment increments due to RCS jet interactions. (*a*) rolling moment due to aft yaw jets, (*b*) side fore due to aft yaw jets. Comparison of flight data from STS-1 (○) and -2 (□) with data book predictions (P) and variations (V) (Kanipe 1983).

enabled extraction of aerodynamic characteristics for flight conditions from continuum to free molecule flow. Analysis of the resulting flight data has yielded an improved bridging formula for use in predicting L/D in the rarefied flow régime (Blanchard & Buck 1986). Whereas the early flight data suggested a partially specular free molecule surface accommodation model, further analysis of multiple flights now supports a near diffuse model. In a further analysis of these data, Blanchard and his co-workers have also shown that, at rarefied-flow flight conditions, the aero data book techniques significantly under-predicted basic vehicle pitching moment and elevon effectiveness and that these underpredictions increased with increasing altitude (Blanchard & Hinson 1989). An interesting and significant spin-off of the HIRAP measurements was the identification of large scale (up to $\pm 60\,\%$) density shears in the Earth's thermosphere which significantly affected the interpretation of the Shuttle flight data (Blanchard *et al.* 1989).

(ii) *Heating*

The prediction of aerodynamic heating rates for the Shuttle Orbiter was accomplished primarily through wind tunnel tests. Since the Orbiter flies at high angles of attack throughout most of the entry heat pulse, the windward and leeside flow fields are fundamentally different. With the exceptions of the control surfaces and the wing leading edge, the windward flow field can be modelled as an inviscid, attached flow over a thin boundary layer. The leeside flow, however, is largely separated and dominated by viscous effects and vortices. Hence, with the notable exceptions of the control surfaces and the wing leading edge, the simulation problem is more difficult for the leeside. Fortunately, except for local vortex impingement regions on the fuselage side and the OMS pods, leeside heating rates are generally low.

In the Shuttle programme, the general approach for the windward heating was to use real-gas boundary layer solutions for simple geometrical shapes (i.e. spheres, wedges, cones, swept cylinders) adjusted to agree with wind tunnel results. The adjustments accounted primarily for streamline divergence and boundary layer running lengths (Haney 1983). Except for the influence of TPS surface catalyticity, this approach was generally successful.

PHILOSOPHICAL TRANSACTIONS OF THE ROYAL SOCIETY A MATHEMATICAL, PHYSICAL & ENGINEERING SCIENCES

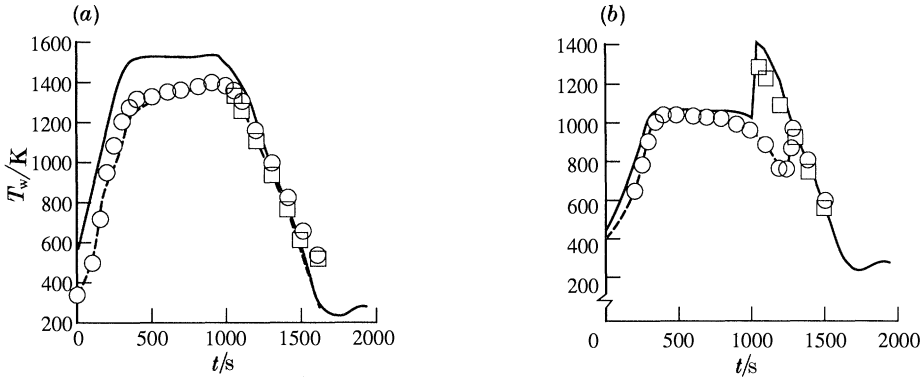

Figure 17. Shuttle windward centre line surface temperatures. (*a*) $x/L = 0.025$, (*b*) $x/L = 0.7$. Comparison of flight data for STS-1 (□) and -2 (○) with predictions assuming equilibrium (——) and finite wall catalycity (– – – –) (Haney 1983).

Early in the Shuttle programme, the decision was made to design the TPS under the assumption of fully catalytic surfaces. At high altitudes, where collision rates are relatively low, it is possible that the dissociated boundary layer species will not reach an equilibrium state of recombination at the TPS surface. This is particularly true if the surface material is non-catalytic with regard to atom recombination. When less than equilibrium recombination occurs, the result is reduced aerodynamic heating. The Shuttle tiles were known to be non-catalytic. However, there was concern that they would not retain their low catalytic efficiency under operational conditions. Hence the Shuttle was conservatively designed to withstand equilibrium heating rates. It was no surprise, then, that heating rates measured during the orbital flight tests were less than equilibrium values. The Shuttle data are, however, the first fully documented flight demonstration of heating rate reduction due to wall non-catalyticity. As such it has significant implications for the design of future hypersonic vehicles.

Representative lower surface heating flight results are presented and compared with various prediction techniques in figures 17–21. In figure 17*a* surface temperature data for a point on the fuselage centreline near the high angle-of-attack stagnation point ($x/l = 0.025$) are compared with predictions using pre-STS-1 methods. While the variation with time is relatively well predicted, the magnitudes are too high for times before approximately 1300 s. In a subsequent discussion, this will be shown to be due primarily to surface catalycity effects. In figure 17*b* data are presented for a downstream location ($x/L = 0.7$). Again, surface temperatures are overpredicted (due to wall catalycity effects) before about 1300 s. Transition was predicted to occur near 1000 s and while the data from STS-1 appear to agree fairly well with this prediction, the STS-2 data indicate transition occurring later near 1200. Actually, the STS-1 result was apparently caused by a gauge in a TPS tile on the nose-wheel door and was atypically early. The STS-2 result is more typical of the transition data as a whole. In the later stages of entry, when the heating is no longer affected by wall catalycity and the boundary layer is fully turbulent, surface temperatures are well predicted. This was true of all the Shuttle data. When the boundary layer was fully turbulent, state-of-the-art boundary-layer theory yielded good predictions when boundary-layer edge conditions were carefully defined (Sutton *et al.* 1988).

Wall catalycity effects are illustrated in figures 18 and 19. In figure 18, windward

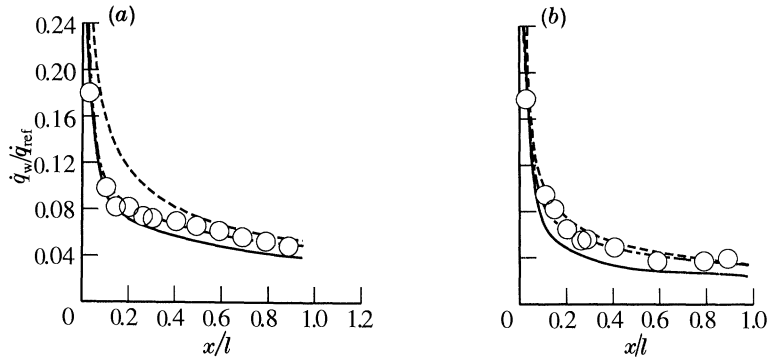

Figure 18. Shuttle windward centre line heating rates. (*a*) $h = 71.3$ km, $M_\infty = 23.4$, $\alpha = 39.4°$, STS-2, (*b*) $h = 57.9$ km, $M_\infty = 14$, $\alpha = 40.9°$, STS-3. Comparison of flight data (○) with viscous shock layer predictions assuming chemical equilibrium (– – –), and finite recombination rates at the wall with $\bar{k}$ from Scott (1981) (——) and $\bar{k}_w$ from Zoby *et al.* (1985) (— - —) (Sutton *et al.* 1988).

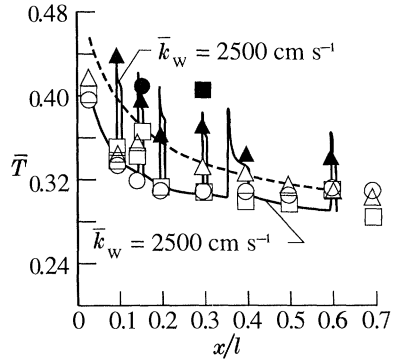

Figure 19. Shuttle windward centreline heating rates with finite wall catalycity. Comparison of flight data for STS-2 (○, ●), -3 (□, ■) and -5 (△, ▲) with theoretical predictions assuming $\bar{k}_w = 100$ cm s^{-1} for uncoated tiles and $\bar{k}_w = 2500$ cm s^{-1} for catalytically coated tiles (——); and chemical equilibrium (– – –) (Stewart *et al.* 1983).

centreline flight data are compared with equilibrium and finite rate predictions at altitudes of approximately 74 and 58 km. The finite rate results were computed using a viscous shock layer code (Shinn *et al.* 1983) and two different sets of oxygen recombination rate coefficients, $\bar{k}_w$. The rate constants of Scott (1981) were measured in arc jet tests at surface temperatures somewhat different from the flight values. Those of Zoby *et al.* (1985) were determined from a 'best fit' to the STS-2 flight data. As figure 18 shows, the flight data are well below the equilibrium predictions at 74 km and are approaching the equilibrium values at 58 km. Both finite rate predictions give significantly improved agreement with the flight data with the acr-jet derived rate coefficients underpredicting the flight results somewhat.

As part of the NASA Orbiter Experiments Program a highly catalytic overcoat was applied to selected windward surface TPS tiles on the Orbiter *Columbia*. By comparing detailed, finite rate boundary layer predictions with measured surface temperatures, Stewart *et al.* (1983) have shown conclusively that the lower heating experienced by the Shuttle is due to wall non-catalycity. An example is presented in figure 19.

The temperature spikes are the predicted result of higher local heating rates

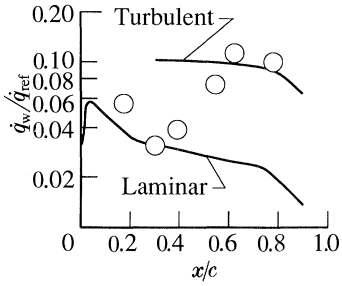

Figure 20. Streamwise windward surface heating-rate distribution on the Shuttle wing at $2y/b = 0.8$. Comparison of STS-2 flight data for $h = 47.9$ km, $M_\infty = 9.15$, $\alpha = 34.8°$ (○) with predictions using an axisymmetric analogue boundary technique (——) (Sutton *et al.* 1988).

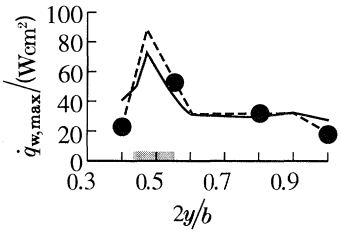

Figure 21. Shuttle wing leading edge heating. Comparison of estimated maximum leading edge temperatures for STS-2, -3, and -5 (– – –) with pre-flight predictions (——). Symbols indicate flight radiometer data. Shading indicates predicted region of highest heating (Cunningham & Haney 1983).

produced by the highly catalytic overcoated tiles. The agreement between theory and the flight measurements is very convincing.

When the Shuttle was being designed, there were no CFD codes capable of predicting the complete, high angle of attack, windward flow field. Such codes do exist now, however, and good success has been achieved in predicting heating for the wings as well as the fuselage. A typical comparison between such predictions and STS-2 flight data is shown in figure 20.

The CFD technique employed uses the HALIS code (Weilmuenster & Hamilton 1983) to compute the inviscid flow field which in turn provides the boundary-layer edge conditions for an axisymmetric-analogue, streamline-following boundary-layer solution (Hamilton *et al.* 1987). The heating shown in figure 20 is for an outboard region of the wing (80% semi-span) and is typical of a flow undergoing transition from laminar near the leading edge to turbulent aft of the 60% chord location. Agreement is acceptable in the fully laminar and fully turbulent regions.

As pointed out previously, prediction of heating to the Orbiter wing leading edge was complicated by the interaction of the bow shock with the leading edge flow field. While the remainder of the leading edge was modelled as a swept cylinder, the prediction of heating in the shock interaction region was based on wind tunnel measurements adjusted by scaling correlations that took into account the nature of the shock interaction (Edney type V) and the influence of shock density ratio (Cunningham & Haney 1983). As is shown in figure 21, the predicted location and magnitude heating appears to be in fair agreement with flight results.

The leading edge instrumentation was sparse, however, consisting of four radiometers which measured the backside temperature of the carbon–carbon leading

PHILOSOPHICAL TRANSACTIONS OF THE ROYAL SOCIETY A MATHEMATICAL, PHYSICAL & ENGINEERING SCIENCES

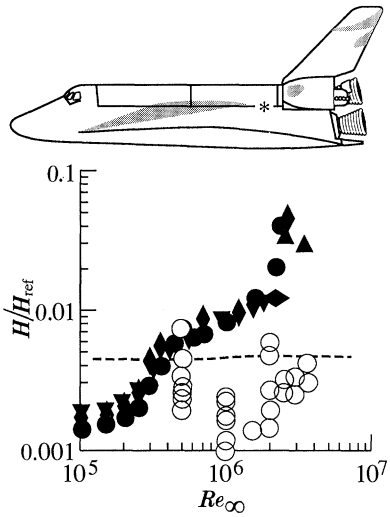

Figure 22. Shuttle orbiter fuselage side heating. Comparison of flight data from STS-1 (◆), -2 (⧫), -3 (▼), -4 (▲), and -5 (●) with wind tunnel data (○) and pre-flight prediction method (– – – –). Shaded region indicates vortex scrubbing. ∗ indicates measurement location (Haney 1983).

edge. A significant underprediction of peak heating may have occurred but the measurements are too few to definitely establish this. Predicting shock interaction effects for hypersonic vehicles remains a challenging task.

While windward heating is, for the most part, amenable to modern analysis techniques, leeside heating remains largely unpredictable. Complete simulation would require simultaneous matching of flight Reynolds number and Mach number as well as non-equilibrium flow field chemistry. The inherent scaling limitations of ground based test facilities make this unachievable. Hence approximate simulations are attempted. In the Shuttle programme, the approach used was to develop correlations of a dimensionless film heat transfer coefficient ratio as a function of angle-of-attack, angle of sideslip, free stream Reynolds number and free stream Mach number. The film coefficient ratio was the ratio of the local film coefficient to that at the stagnation point of a 0.3 m radius sphere. This essentially correlated the Orbiter leeside heating in terms of blunt-body relations. In comparing flight results with predictions, a distinction must be drawn between those regions of the Orbiter surface subject to vortex scrubbing (i.e. portions of the fuselage side, OMS pads, vertical tail and wing upper surface downstream of the leading-edge shock interaction region) and those regions subjected to separated flow. In the separated flow regions (the fuselage centreline and most of the wing upper surface) the flight heat transfer rates were very low, in general less than 1% of the reference values. These heating rates were for the most part, lower than those predicted from ground test results. This was apparently due to laminar-to-turbulent transition in the separated flow having occurred at a much lower Reynolds number in the wind tunnels than in flight (Throckmorton & Zoby 1983). In those regions subject to vortex scrubbing, the heat transfer rates were considerably higher, approaching 10% of the reference values. The surface regions subject to the most important vortex scrubbing are illustrated schematically in figure 22.

Figure 22 also presents a comparison between wind tunnel and flight results for a point on the fuselage side upstream of the OMS pad. Note that the correlation

technique was not successful in predicting either the magnitude or the trend of the flight data, and seriously underpredicted the heating at the higher Reynolds numbers. At present, the prediction of the location of leeside vortex impingement and the resultant heating remains an imprecise art.

(iii) *Boundary-layer transition*

It was pointed out in discussing Reentry F that a large body of flight data exists for boundary layer transition on conical vehicles. The overall trends of this data set in terms of local transition Reynolds number and boundary edge Mach number are displayed in figure 11. The range of the Shuttle windward centreline transition data is also displayed for comparison. It may seem inappropriate to compare the Shuttle and cone data-sets since the vehicle configurations are very different. Certainly there are important differences but it should be recalled that the flow field along the Orbiter windward centreline is closely approximated by the axisymmetric flow over a cone with a half-angle approximately equal to the Orbiter's angle of attack (Woods *et al.* 1983). As shown in figure 11, local Mach numbers along the Shuttle windward centreline range from approximately 1.5–2.5, complement the cone data, and fit into the gross trend of transition Reynolds number increasing with local Mach number. Also, like the cone data, the range of observed transition Reynolds number, at a given Mach number is almost an order of magnitude, suggesting that some other transition criteria, such as a roughness Reynolds number or a momentum thickness Reynolds number might better correlate the flight data. In the case of the cone data many different criteria have been tried but none has been truly successful (Berkowitz *et al.* 1977). The Shuttle data, on the other hand exhibit markedly reduced scatter when plotted in terms of a roughness Reynolds number Re_k based on conditions at the height of the misaligned tiles, k. This is shown in figure 23*a*.

The data from flights STS-2, 3 and 5 coalesce nicely. STS-1 experienced an anomalously early forward movement of transition caused by a large gauge in one of the tiles on the nose-wheel-well door. The reason for the derivation of the STS-4 data is not well understood. Overall, however, figure 23*a* suggests a near constant value for $Re_{k,T}$ for points downstream of $x/L = 0.2$. Upstream of $x/L = 0.1$, the nose curvature produces a strong favourable pressure gradient which stabilizes the boundary layer. Hence, larger values of $Re_{k,T}$ are required in this region. Figure 23*b* shows the rapid forward movement of transition that characterizes the Shuttle data. Flights STS-2 to STS-5 all exhibited similar behaviour. STS-1 exhibited a more gradual movement of the transition front, apparently caused by the previously mentioned tile damage. As pointed out by Goodrich *et al.* (1983) and Poll (1986), this rapid forward movement is characteristic of transition dominated by large scale surface roughness. Figure 23 also shows that wind tunnel data underpredicted transition Reynolds numbers and times for $x/L \gtrsim 0.4$. This is undoubtedly due to wind tunnel noise. The good agreement shown for $0.1 < x/L < 0.2$ suggests that transition in this region was dominated by surface roughness and shock layer phenomena (rather than noise) in the tunnel tests as well as in flight. This conclusion is further supported by figure 23*b*. In discussion of roughness-dominated transition, reference is often made to the 'incipient', 'critical', and 'effective' values of roughness Reynolds number. Roughness first begins to cause derivations from smooth wall behaviour at the incipient value. Rapid forward movement of transition begins at the critical value and at the effective value, the transition front stabilizes near the disturbance-generating roughness element. Pre-flight wind tunnel tests had

PHILOSOPHICAL TRANSACTIONS OF THE ROYAL SOCIETY A MATHEMATICAL, PHYSICAL & ENGINEERING SCIENCES

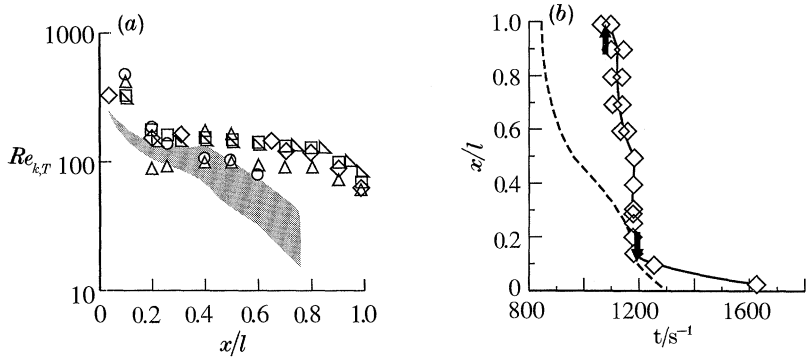

Figure 23. Shuttle boundary layer transition data. (*a*) roughness Reynolds number at transition onset from STS-1 (○), -2 (□), -3 (◇), -4 (△), and -5 (◺) compared with wind tunnel data (shaded region), (*b*) transition times from STS-3 (—◇—) compared with wind tunnel based predictions (– – –). ↑ indicates Re_k; ↓ indicates effective Re_k (Goodrich *et al.* 1983).

established respective incipient, critical, and effective values 30, 110, and 180 for Re_k at $x/L = 0.1$ (Goodrich *et al.* 1983). The arrows shown in figure 23*b* show the times at which $Re_k = 110$ and 180 based on flight for STS-3. Good agreement, like that shown in figure 23*b*, was achieved for STS-2 to 5.

7. Validated design techniques

Overall, the flight test programmes discussed in this paper demonstrate the feasibility of designing hypersonic vehicles based on tests in conventional perfect-gas wind tunnels supplemented by state-of-the-art CFD analyses. The X-15, Asset, Prime and Shuttle vehicles all performed essentially as predicted. At Mach numbers up to approximately 8, real-gas effects are small and Mach number/Reynolds number simulation is sufficient to insure accurate prediction of aerodynamic characteristics. At Mach numbers greater than 8, real-gas effects become important but appear to affect primarily pitching moment (hence longitudinal trim) and to have little effect on other aerodynamic characteristics. Viscous interaction effects are relatively small and occur only at high altitudes, but can have a significant impact on hypersonic axial force predictions. They appear to be well correlated by the viscous interaction parameter $\bar{V}'_\infty$.

Stability and control derivatives, with the exception of RCS jet interaction derivatives, appear to be predicted throughout the hypersonic speed range by conventional wind-tunnel test techniques. Overall, with the notable exceptions of longitudinal trim and jet interaction effects, it appears that the configuration aerodynamics of hypersonic vehicles can be accurately predicted by perfect-gas wind tunnel tests. This also implies that chemically reacting CFD codes (which can consume large amounts of computer resources) may be needed only for selected real-gas design issues so that the major part of a vehicle design effort can use perfect-gas analyses.

State-of-the-art aerodynamic heating techniques appear to give accurate predictions for laminar and fully turbulent heating for attached flows so long as there are no strong shock interaction or non-equilibrium chemistry effects. For such attached, shock-free, equilibrium flows, heating rate distributions appear to depend only weakly on Mach number for $M \gtrsim 8$. Hence wind tunnel tests at $M \approx 8$–10 can

be used to predict heating rate distributions at high hypersonic Mach numbers. Also for such flows, modern compressible boundary-layer theory appears to yield good heating predictions so long as accurate, high-temperature thermodynamic and transport properties and carefully defined edge conditions are used. It should be noted, in this regard, that the definition of accurate boundary layer edge conditions may require streamline-following techniques and detailed inviscid flowfield computations. The alternatives, of course, are viscous shock layer solutions or Navier–Stokes solutions.

For high altitude flows with dissociation, surface catalycity effects can significantly influence heating levels. Modern, finite-rate boundary layer analyses using the best available surface recombination rate data are capable of predicting major heating trends but further work on accurately measuring recombination rate coefficients is needed.

8. Remaining challenges

The accurate prediction of longitudinal trim remains a problem. It seems clear that real-gas effects must be accounted for and scaling constraints make this difficult in ground based test facilities. It has been suggested that tests in perfect-gas wind tunnels which use non-air test gases (i.e. CF_4) chosen to produce flight levels of shock density ratio may provide adequate simulation. Much work remains to be done to prove the reliability of this test technique. A detailed, finite rate, Navier–Stokes (or Euler) solution for a complex vehicle geometry can tax even the most powerful computers. There are indications that inviscid, equilibrium chemistry solutions may suffice thus making the computing task tractable (though still large). The hypersonic longitudinal trim problem is an area worthy of serious attention.

Predicting of effectiveness of blended control system during the early stages of re-entry poses similar problems. There are no obvious solutions to the scaling problem in ground based facilities and, because complex, separated, viscous dominated flows are involved, computational solutions would tax present computers.

The prediction of shock interaction heating remains an important, unsolved problem. While CFD solutions for simple geometries exist, complex flows, like the Shuttle leading edge shock interaction region remain beyond the capability of current analytical or experimental techniques. It should be remembered that, in all likelihood, this phenomena produced the highest heating rates on the Shuttle Orbiter.

While the heating rates involved are generally low, an even greater complexity and lack of capability exists for separated and vortex-dominated leeside flows. Vortex scrubbing, like that on the Shuttle fuselage sides and OMS pods, can produce heating rates comparable to windward side values. The leeside heating problem is also non-trivial. It has been estimated that, because of necessary design conservatism, the Shuttle Orbiter *Columbia* carried up to 500 kg of unneeded leeside TPS.

Even more serious is the continuing inability to predict boundary-layer transition in flight. While the total flight data base is relatively large, it appears that transition on the flight vehicles is governed by so many different phenomena that only small subsets of the data, over limited flight régimes, are truly comparable. Hence, attempts to find overall correlating parameters have proved largely futile. The Shuttle transition data set is extensive and fairly definitive but appears to be applicable only to Shuttle-like vehicles with large surface roughness. Hence it may be of little help to designers of airbreathing launch vehicles.

PHILOSOPHICAL TRANSACTIONS OF THE ROYAL SOCIETY A MATHEMATICAL, PHYSICAL & ENGINEERING SCIENCES

Finally, it must be pointed out that there are no hypersonic flight data on the propulsion–airframe integration effects that are so important for airbreathing launch vehicles. Real-gas effects may strongly influence theses flows, especially with regard to nozzle efficiency and thrust vectoring. Shock interaction and vortex impingement heating could be very important for these vehicles and the prediction of turbulent transition and subsequent relamarization may be a crucial design issue.

9. Concluding remarks

Over the past 30 years a sizeable body of hypersonic flight experience has accumulated. The fundamentals of hypersonic flight are well understood. Many lessons have been learned and a few myths have been exploded. The ability to successfully design and fly hypersonic re-entry gliders has been convincingly demonstrated, albeit with a considerable degree of conservatism, by the X-15, Asset and Prime, the Shuttle Orbiter and Buran. While important research on this class of vehicle remains to be done, the key phenomena are understood. Much of this knowledge is directly applicable to airbreathing launch vehicles and hypersonic aircraft, but there are crucial design issues (like airframe–propulsion integration) where there is no flight experience. These problems are formidable but certainly no more daunting than those faced by the X-15 team in 1954. The flight experience of the past 30 years provides a secure footing for the next steps in hypersonic flight.

References

Arrington, J. P. & Jones, J. J. (eds) 1983 Shuttle performance: lessons learned. *NASA Conf. Publ.* 2283, parts 1 and 2.

Banner, R. D., Kuhl, A. E. & Quinn, R. D. 1962 Preliminary results of aerodynamic heating studies on the X-15 airplane. *NASA TM X-638.*

Becker, J. V. 1969 The X-15 program in retrospect. *Raumfahrtforschung Heft* **2/69**, 45–53.

Beckwith, I. E. & Bartram, M. H. 1972 A survey of NASA Langley studies on high speed transition and the quiet tunnel. *NASA TM X-2566.*

Berkowitz, A. M., Kyriss, C. L. & Martellucci A. 1977 Boundary layer transition flight test observations. *AIAA paper 77–125.*

Blanchard, R. C. & Buck, G. M. 1986 Rarefied-flow aerodynamics and thermosphere structure from Shuttle flight measurements. *J. Spacecraft Rockets* **23**, 18–24.

Blanchard, R. C. & Hinson, E. W. 1989 Flight measurements of Shuttle orbiter pitching-moment coefficient and elevon effectiveness in the rarefied flow regime. *NASA TP 2889.*

Blanchard, R. C., Hinson, E. W. & Nicholson, J. Y. 1989 Shuttle high resolution accelerometer package experiment results: atmospheric density measurements between 60 and 160 km. *J. Spacecraft Rockets* **26**, 173–180.

Chaffee, N. (ed.) 1985 Space Shuttle technical conference. *NASA Conf. Publ.* 2342, parts 1 and 2.

Compton, H. R., Schiess, J. R., Suit, W. T., Scallion, W. I. & Hudgins, J. W. 1983 Stability and control over the supersonic and hypersonic speed range. Shuttle performance: lessons learned. *NASA Conf. Publ.* 2283, part 1, pp. 473–508.

Cunningham, J. A. & Haney, J. W. 1983 Space Shuttle wing leading edge heating environment prediction derived from development flight data. Shuttle performance: lessons learned (ed. J. P. Arrington & J. J. Jones). *NASA Conf. Publ.* 2283, part 2, pp. 1083–1109.

Goodrich, W. D., Derry, S. M. & Bertin, J. J. 1983 Shuttle orbiter boundary layer transition at wind tunnel conditions. Shuttle performance: lessons learned (ed. J. P. Arrington & J. J. Jones). *NASA Conf. Publ.* 2283, part 2, pp. 753–779.

Hallion, R. P. 1983 The path to Space Shuttle: the evolution of lifting reentry technology. *J. Brit. Interplanetary Soc.* **36**, 523–541.

Hallion, R. P. 1987 *The hypersonic revolution: eight case studies in the history of hypersonic technology*, vol. 1 (from Max Valier to Project Prime). Ohio, U.S.A.: USAF Aeronautical Systems Division.

Hamilton, H. H., DeJarnette, F. R. & Weilmuenster, K. J. 1987 Application of axisymmetric analogue for calculating heating in three-dimensional flow. *J. Spacecraft Rockets* **24**, 296–302.

Haney, J. W. 1983 Orbiter entry heating lessons learned from development flight test program. Shuttle performance: lessons learned. *NASA Conf. Publ.* 2283, part 2, pp. 719–753.

Kanipe, D. B. 1983 Plume/flowfield jet interaction effects on the Space Shuttle orbiter during entry. *J. Spacecraft Rockets* **20**, 351–355.

Keener, E. R. & Pembo, C. 1962 Aerodynamic forces on components of the X-15 airplane. *NASA TM X-712*.

Maine, R. E. & Iliff, K. W. 1980 User's manual for the MMLE-3, a general fortran program for maximum likelihood parameter estimation. *NASA TP-1563*.

Maus, J. R., Griffith, B. J., Szema, K. Y. & Best, J. T. 1984 Hypersonic Mach number and real gas effects on Space Shuttle orbiter aerodynamics. *J. Spacecraft Rockets* **21**, 136–141.

Poll, D. I. A. 1986 A new hypothesis for transition on the windward face of the Space Shuttle. *J. Spacecraft Rockets* **23**, 605–611.

Powell, J. W. & Hengeveld, E. 1983 Asset and Prime: gliding reentry test vehicles. *J. Brit. Interplanetary Soc.* **36**, 369–376.

Pyle, J. S. 1964 Comparison of flight pressure measurements with wind-tunnel data and theory for the forward fuselage of the X-15 airplane at Mach numbers from 0.8 to 6.0. *NASA TN D-2241*.

Pyle, J. S. 1965 Flight-measured wing surface pressures and loads for the X-15 airplane at Mach numbers from 1.2 to 6.0. *NASA TN D-2602*.

Rockwell International Space Division 1980 Aerodynamic design data book, vol. 1: orbiter vehicle, final report. *NASA CR 160903*.

Romere, P. O., Kanipe, D. B. & Young, J. C. 1983 Space Shuttle aerodynamic comparisons of flight 1 with preflight predictions, *J. Spacecraft Rockets* **20**, 15–21.

Romere, P. O. & Young, J. C. 1983 Space Shuttle entry longitudinal aerodynamic comparison of flight 2 with preflight predictions. *J. Spacecraft Rockets* **20**, 518–523.

Schlosser, D. C. & Dominik, D. F. 1983 Approach to estimating the effect of aeroelasticity on the aerodynamic characteristics of the Space Shuttle orbiter. Shuttle performance: lessons learned. *NASA Conf. Publ.* 2283, part 1, pp. 309–346.

Scott, C. D. 1981 Catalytic recombination of nitrogen and oxygen on high-temperature reusable surface insulation. In *Aerothermodynamics and planetary entry; progress in astronautics and aeronautics* (ed. A. L. Crosbie), vol. 77, pp. 192–213.

Shinn, J. L., Moss, J. N. & Simmonds, A. L. 1983 Heating analysis for the Shuttle windward plane with surface finite catalytic recombination rates. In *Entry vehicle heating and thermal protection system; space shuttle, solar starprobe, jupiter galileo probe; progress in astronautics and aeronautics* (ed. P. E. Bauer & H. E. Collicott), vol. 85, pp. 149–180.

Stetson, K. F. 1987 On predicting hypersonic boundary layer transition. *AFWAL-TM-84-160-FIMG*. Ohio, USA: USAF.

Stewart, D. A., Rakich, J. V. & Lanfranco, M. J. 1983 Catalytic surface effects on Space Shuttle thermal protection system during earth entry of flights STS-2 through STS-5. Shuttle performance: lessons learned. *NASA Conf. Publ.* 2283, part 2, pp. 827–845.

Stone, J. S. & Baumbach, J. J. 1983 Space Shuttle orbiter reaction control system flight data anomalies. Shuttle performance: lessons learned. *NASA Conf. Publ.* 2283, part 1, pp. 381–395.

Sutton, K., Zoby, E. V. & Hamilton, H. H. 1988 Overview of CFD methods and comparisons with flight aerothermal data. In *AGARD Symposium on Validation of computational fluid dynamics*.

Throckmorton, D. A. & Zoby, E. V. 1983 Orbiter entry leeside heat-transfer data analysis. *J. Spacecraft Rockets* **20**, 524–530.

Weilmuenster, K. J. & Hamilton, H. H. 1982 A comparison of computed Space Shuttle orbiter surface pressure with flight measurements. *AIAA paper 82-0937*.

Weilmuenster, K. J. & Hamilton, H. H. 1983 High angle of attack inviscid flow calculations over Shuttle-like vehicles with comparisons to experimental data. *NASA TP-2103*.

PHILOSOPHICAL TRANSACTIONS OF THE ROYAL SOCIETY A MATHEMATICAL, PHYSICAL & ENGINEERING SCIENCES

Whitnah, A. M. & Hillje, E. R. 1982 Space Shuttle wind tunnel program summary. *AIAA paper 82-0562*.

Woods, W. C., Arrington, J. P. & Hamilton, H. H. 1983 A review of preflight estimates of real-gas effects on Space Shuttle aerodynamic characteristics. Shuttle performance: lessons learned. *NASA Conf. Publ.* 2283, part 1, pp. 309–346.

Wright, R. L. & Zoby, E. V. 1977 Flight boundary layer transition measurements on a slender cone at Mach 20. *AIAA paper 77-719*.

Young, J. C. & Underwood, J. M. 1983 Development of aerodynamic uncertainties for the Space Shuttle orbiter. *J. Spacecraft Rockets* **20**, 513–517.

Zoby, E. V., Gupta, R. N. & Simmonds, A. L. 1985 Temperature-dependent reaction rate expressions for oxygen recombination. In *Thermal design of aeroassisted orbital transfer vehicle: progress in astronautics and aeronautics* (ed. H. F. Nelson) vol. 96, pp. 446–465.

PHILOSOPHICAL TRANSACTIONS OF THE ROYAL SOCIETY A MATHEMATICAL, PHYSICAL & ENGINEERING SCIENCES